

The Necessity of Comparators in Wake-Up Receiver Circuits

Robert Fromm, Olfa Kanoun and Faouzi Derbel

Note: This is the manuscript version of this publication. This article is not yet published.

Current version: May 13, 2024.

Abstract

Wake-up receivers (WuRxs) play a crucial role in enabling wireless sensor nodes to operate efficiently on battery power while ensuring low-latency communication. Typically, comparators are employed to facilitate the conversion from analog to digital signals. However, some recent proposals opt to exclude the comparator to achieve minimal power consumption. This article delves into the investigation of the shoot-through effect present in CMOS devices. Our measurements reveal that connecting analog signals directly to CMOS devices can lead to a significant increase in power consumption, reaching up to a thousandfold. Analyzing our findings in the context of existing research, we project that the shoot-through effect severely limits the battery life of sensor nodes in real-world applications. To address this challenge, we propose the use of nano-power comparators that do not exhibit shoot-through effects. While our proposed comparator circuit adds additional 175 nA of power consumption, it significantly enhances the reliability of various wake-up receivers.

Keywords

Envelope detector, reliable, ultra-low power, wake-up receiver, wireless sensor network.

1 Introduction

Long-lasting battery-powered sensor nodes are essential for ensuring the cost-effectiveness of wireless sensor networks. The design of these sensor nodes revolves around key considerations such as power consumption, response time, and communication range. Notably, even modern RF transceivers demand more than

10 mW to remain in continuous reception mode. To address this high power consumption, a common practice involves reducing idle-listening time through the introduction of duty-cycling behavior. However, it is crucial to note that while this approach helps conserve power, it leads to increased latency. [GD15; Ché+13; Kan+18]

Wake-up receivers (WuRxs), specialized RF receivers, are proposed to maintain continuous reception within sensor nodes. These WuRxs are designed to achieve the lowest possible power consumption. Typically, WuRxs are divided into two categories: those integrated into application-specific integrated circuits (ASICs) and those constructed using commercial off-the-shelf (COTS) components. Our preference is for the utilization of COTS components, driven by the desire for improved repeatability of results, as well as simpler and more cost-effective implementations. [Piy+17]

Figure 1 illustrates the basic building blocks of a low-power WuRx and depicts various signal types involved in the WuRx system. The antenna captures the RF signal, which undergoes conversion to LF through the passive radio-frequency envelope detector (RFED). Usually, an amplifier circuit is utilized to enhance the LF signal. [Piy+17]

This article primarily explores the LF-to-digital converter, the subsequent building block. Analog-to-digital converters or comparators are commonly employed in this role. Certain studies exclude this component and directly input the analog signal into the address decoder circuitry. Typically, the address decoder circuit is digital and produces a digital signal upon detecting a matching wake-up packet [Piy+17].

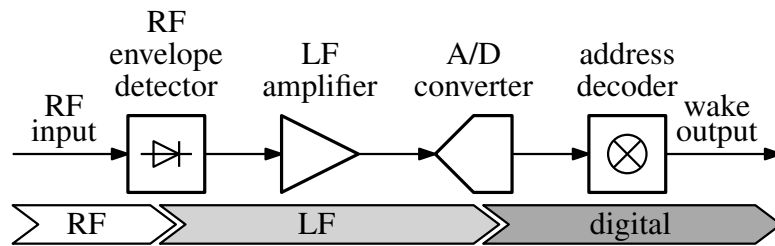


Figure 1: Typical building blocks and signal conversion chain of a low-power wake-up receiver (WuRx).

In this article, we will present measurements of the shoot-through effect (STE) in various complementary metal-oxide-semiconductor (CMOS) devices. The STE occurs when an analog signal with an intermediate voltage is connected to a digital input of a CMOS gate. When a digital signal (near 0 V or near supply voltage) is connected to a CMOS logic gate, only one of the two complementary metal-oxide-semiconductor field-effect transistors (MOSFETs) conduct. However, a interme-

diated input voltage leads to an additional supply current flow because both complementary MOSFETs of the digital gate will go into slight conduction. [HH15, p.760]

The STE is not well-known, and detailed specifications and measurements are not readily available. Therefore, we chose to quantify the STE through measurements on eight different CMOS devices. We observed STE currents of up to 6 mA. When compared to the typical supply currents of WuRxS in the range of 1 μ A, the STE can significantly decrease the battery life of the sensor node.

To mitigate the STE, we proposed an ultra-low power circuit based on a comparator and reference generator. This circuit increases the WuRx's supply current by only 175 nA. However, it ensures that no STE currents occur, thereby increasing the battery life of the sensor node in real-life scenarios.

The article is structured as follows: In section 2, we delve into the state of research regarding COTS-based WuRxS. We emphasize that many implementations directly connect analog signals to CMOS devices. In section 3, we introduce our STE measurement setup and present the results, illustrating that connecting analog signals to CMOS devices leads to high STE currents. In section 4, we propose a circuit to mitigate the STE and discuss its implementation. Finally, in section 5, we provide a summary and conclusion of the article.

2 State of Research

In this section of the article, we highlight COTS-based WuRx implementations that directly connect the analog signal to CMOS devices. The subsequent section will present our measurements, revealing that this practice might result in additional supply currents well beyond the average power consumption of a typical WuRx. Malinowski et al. [Mal+07] propose a sensor node for monitoring exceptional events. As part of its design, there is an RFED operating in the 300 MHz range. The RFED output is amplified by a TLV2401 operational amplifier, with gain adjustable by a digital potentiometer in the range of 20–1000. The output of this amplifier circuit is directly connected to a digital input of the MSP430 microcontroller. In section 3, we conducted measurements to evaluate the STE of an MSP430 with the same supply voltage of 3 V. The STE occurs with an input voltage in the range of 0.7 V to 1.7 V. The output of Malinowski's circuit can reach these levels even without any RF signal, owing to the biased RFED, input offset of the TLV2401 operational amplifier, and the high amplification factor. The resulting STE currents can lead to random battery depletion in a fraction of the devices.

Magno and Benini [MB14] suggested a low-power WuRx by incorporating a com-

parator circuit with an adaptive reference generator at the RFED's output. Sensitivity levels varied depending on the comparator used, achieving -32 dBm for the TLV3691 and -55 dBm for the LPV7215. A passive preamble detector, connected to the comparator's output, generates an analog signal. This wake-up signal is directly linked to the PIC12 microcontroller, potentially causing STE currents. Figure 2 shows the preamble detector with the component values presented in [MB14].

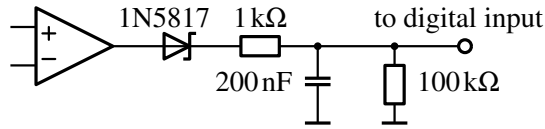


Figure 2: Preamble detector and component values presented in [MB14].

We simulated this preamble detector in LTspice and displayed the input and output signals in Figure 3. To model a noisy comparator output, we employed a random digital signal with a duty cycle of 1:10. At $t = 4$ ms, we introduced a continuous H signal lasting for $350 \mu\text{s}$ to simulate an incoming preamble.

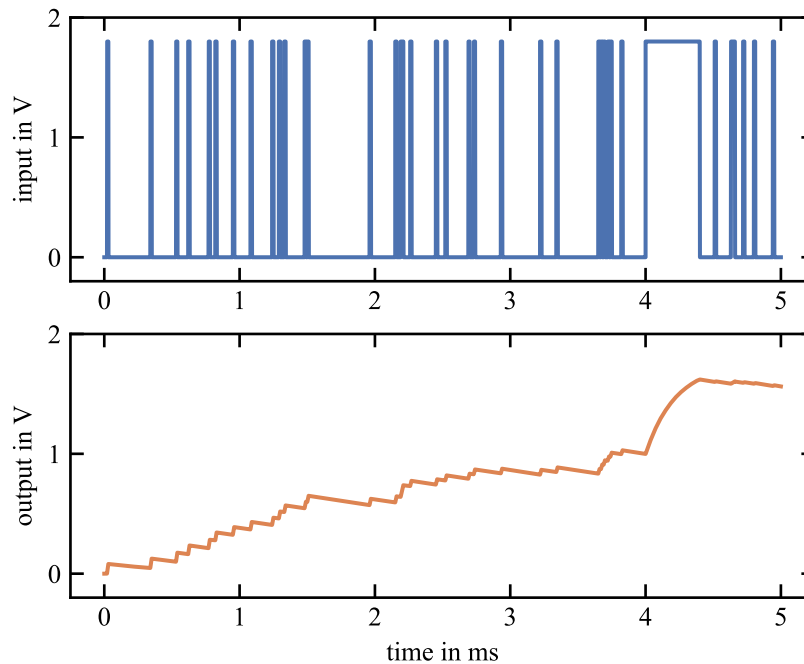


Figure 3: Input and output signal of the preamble detector simulated with LTspice.

The simulation clearly indicates that even in low-noise environments, the preamble detector produces intermediate voltages on its output. Since the preamble detector's output is directly connected to the microcontroller's digital input, the shoot-through effect is highly likely. For the PIC12 microcontroller, we measured shoot-through currents up to $30 \mu\text{A}$ at a supply voltage of 2.0 V. This represents

a 40-fold increase compared to the LPV7215-based proposal in [MB14]. A sensor node designed for a 10-year battery life might only last for 150 days.

The preamble detection circuit presented in [MB14] has been utilized by multiple other WuRx articles. We found evidence in more than 20 articles that this circuit was used. The following list is a selection of these articles, naming each first author only once: [Del+16; Gom+18; GFL19; Frø+19; SMN20; Dji+21; Pol+22; Ben+22; LP22].

3 Shoot-Through Effect Measurements

3.1 Measurement Setup

Our setup for the STE measurements is shown in Figure 4. The device under test (DUT) was connected to two different DC voltage sources generated by the DG1022Z signal generator. V_{CC} represents the supply voltage, and V_{IN} is the input voltage connected to the digital input of the DUT. Both currents flowing into the pins I_{CC} and I_{IN} were measured with the 34450A digital multimeter. Directly analyzing the output voltage of the DUT with an oscilloscope is not possible. The typical oscilloscope probe impedance of 1 M Ω or 10 M Ω will create a significant current flow and increases the I_{CC} measurement. We ensured that the output of the DUT stays unloaded by buffering the output with a comparator. We chose a fixed reference voltage of 0.3 V and supplied the comparator with 3 V. For devices with multiple inputs, only a single input was investigated. All the unused inputs of the DUT were connected to ground.

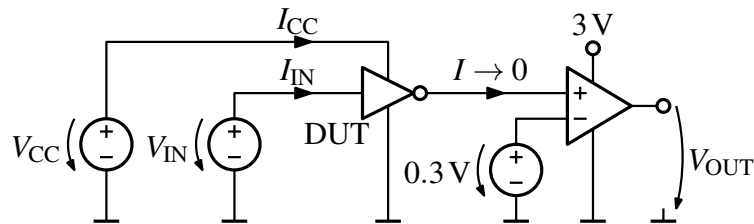


Figure 4: Setup for shoot-through effect measurements.

A measurement involves stepping through the specified input voltage range of the DUT in both rising and falling directions. This is done to account for the hysteresis of the input characteristic and to detect both points where the output latches (trip points). We conducted multiple measurements for each device at various supply voltage levels as per the specifications. We did not supply voltages above 3 V since this is typically the upper limit for WuRx applications.

3.2 Device Selection

According to [HH15], the STE occurs only in the input stage of the CMOS device. We have therefore chosen the simplest form of CMOS gate, the inverter. In most logic families, inverters have two different input characteristics. CMOS input devices have the designator '04 and Schmitt trigger inputs have the designator '14 [HH15, p. 716]. We also decided to investigate the HC, LV and AUP logic families. The HC family is commonly used for logic gates. However, its lower voltage limit is high with 2 V. The LV family has a lower voltage limit of 1.2 V and has been introduced more recently. The AUP family has the lowest voltage limit of 0.8 V and is supplied with single gate devices. [HH15, p. 706]. Both features render the AUP family ideal for use in WuRx circuits.

In addition, we decided to investigate the input stages of two different microcontrollers. As mentioned in the state of research section of this article, the MSP430 and PIC12 are ideal for the WuRx applications due to their low power consumption. We chose the devices with part numbers MSP430G2553 and PIC12LF1572.

3.3 Measurement Results

Figure 5 shows the measurement results for the SN74HC14 CMOS inverter with Schmitt trigger inputs. The measurements were performed with three different supply voltages and are displayed in three different colors. The forward measurements with rising input voltage are shown as solid traces. The reverse measurements with falling input voltage are the dashed traces. The trip points are marked with dots. Because of the hysteresis, there are two different trip points. The right dot is always the forward trip point and the left dot is the reverse trip point. The upper plot shows the variation of the supply current I_{CC} over the input voltage V_{IN} . The lower plot shows the variation of the input current I_{IN} over V_{IN} . At input levels near the supply rails ($V_{IN} = 0$ or $V_{IN} = V_{CC}$), the supply current is less than 100 nA. However, two different effects cause the supply current to rise above this level. First, the clamping current of the input protection circuit allows current to flow from the input pin through the supply pins. This effect is seen in both currents and opposite directions.

Second, the STE is seen with intermediate input voltages. A significant increase in supply current can be seen. It is important to note that the input currents are not affected by the STE. Due to the internal hysteresis, the STE currents depend on the trip points. The highest STE currents are reached near the trip points and at higher supply voltages. For the SN74HC14 device, we measured a maximum supply current of 248 μ A. Since the input current curves I_{IN} are similar for all

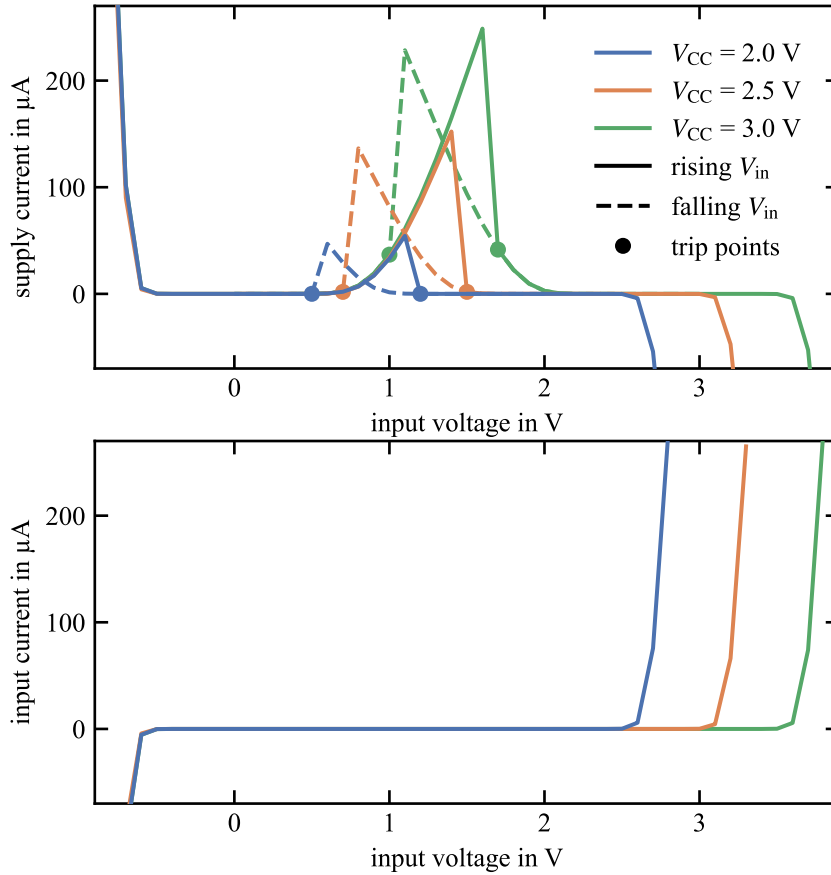


Figure 5: Supply and input current of SN74HC14 CMOS inverter with Schmitt trigger inputs.

devices and these curves do not represent the STE, we will only show the supply current curves I_{CC} from now on. Please see the data availability statement at the end of this article for access to the full data set.

Figure 6 shows the measurement results of the SN74HC04 inverter with CMOS inputs. In general, this device shows almost the same STE currents as the SN74HC14 with Schmitt trigger inputs. We measured a maximum STE current of $189 \mu\text{A}$.

The measurement results of the two LV family devices are shown in Figure 7 and Figure 8. The 74LV14 show similar curves to the previous family. The STE currents increase to $310 \mu\text{A}$. The 74LV04 device with CMOS inputs shows significantly different behavior and narrower trigger points. However, the 74LV04 shows strong STE currents up to 6.0 mA in the reverse path. At 1.0 V supply voltage, both devices show very low STE currents of $2.2 \mu\text{A}$ and $0.7 \mu\text{A}$, respectively.

The measurement results of both devices of the AUP family are shown in Figure 9 and Figure 10. Both devices behave similarly to the LV family. The SN74AUP2G14 device with Schmitt trigger inputs shows the typical M-shaped figures. The STE currents here are increased to $250 \mu\text{A}$. The SN74AUP2G04 device shows narrow

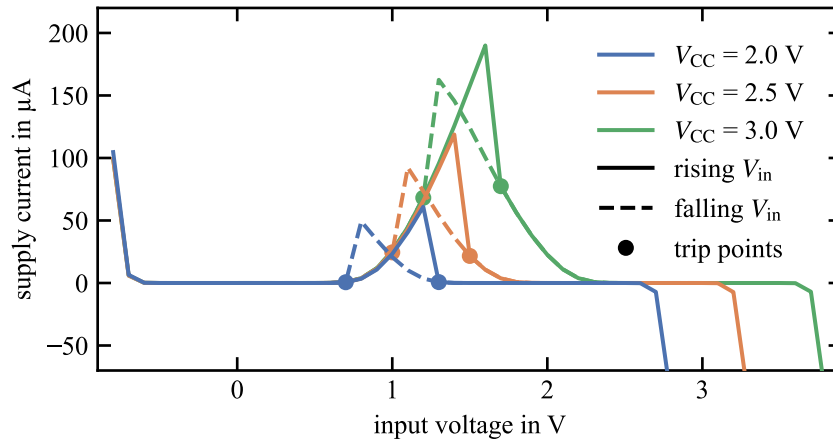


Figure 6: Measurement results for SN74HC04 CMOS inverter.

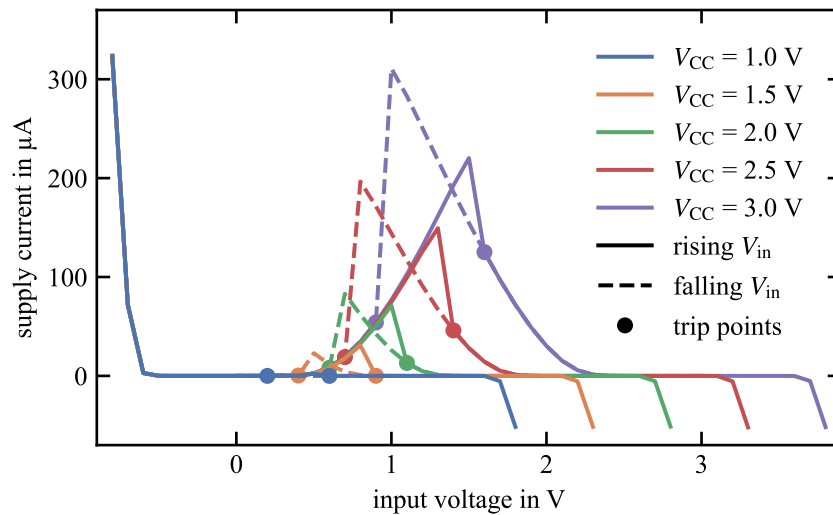


Figure 7: Measurement results for 74LV14 CMOS inverter with Schmitt trigger inputs.

trip points and high STE currents. The STE currents reached a maximum of 3.1 mA when supplied with 2.5 V. The STE currents at 1 V are 8.3 μA and 0.6 μA , respectively.

For both microcontrollers, a single pin was configured as an input and the pin interrupt was enabled. The microcontroller entered the lowest possible power saving mode. Another pin was defined as output and was toggled whenever the input changed and the interrupt occurred. The measurement results of the two investigated microcontrollers are shown in Figure 11 and Figure 12. Both show a slightly different behavior compared to the M-shaped figures of the previous devices (see Figure 5, Figure 7 and Figure 9). The maximum STE currents are at least a factor of three smaller than those of the investigated logic gates. The maximum STE currents of the MSP430G2553 reached 17 μA at 1.8 V and 83 μA at 3.0 V. The maximum STE currents of the PIC12LF1572 reached 34 μA when

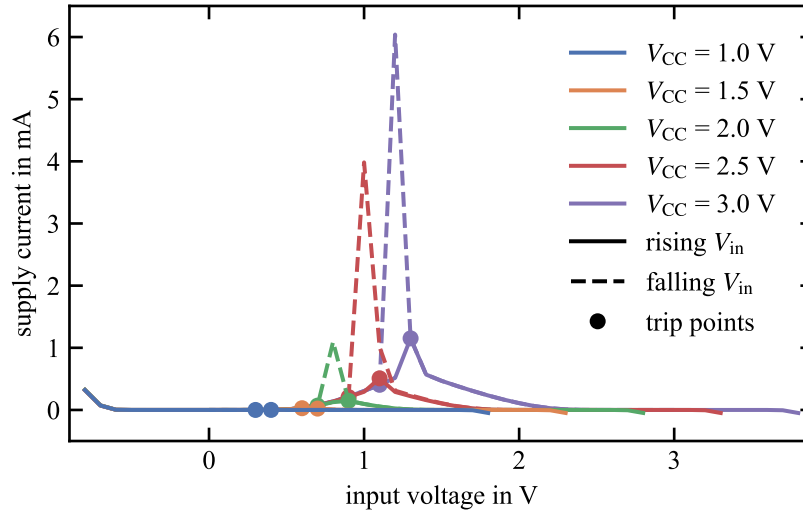


Figure 8: Measurement results for 74LV04 CMOS inverter.

supplied with 2.0 V and 84 μ A at 3.0 V.

We can conclude that the STE greatly increases the supply current of CMOS devices. We have found that for most devices and supply voltages the STE currents are greater than 10 μ A. Therefore, the power consumption of a WuRx implementation is increased by at least a factor of 10 when the STE occurs. Whether the input voltage is in the range where the STE occurs depends on the circuit. However, with real-world factors such as noise or the input offset voltage of the LF amplifier, it becomes increasingly likely that a fraction of the WuRx-equipped sensor nodes will experience faster battery depletion. To mitigate these effects, we proposed the shoot-through avoidance circuit, which is presented in the following section.

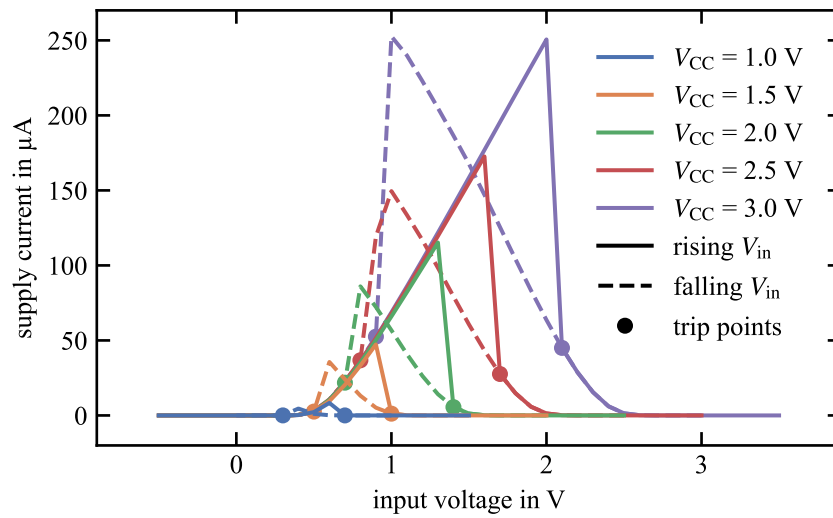


Figure 9: Measurement results for SN74AUP2G14 CMOS inverter with Schmitt trigger inputs.

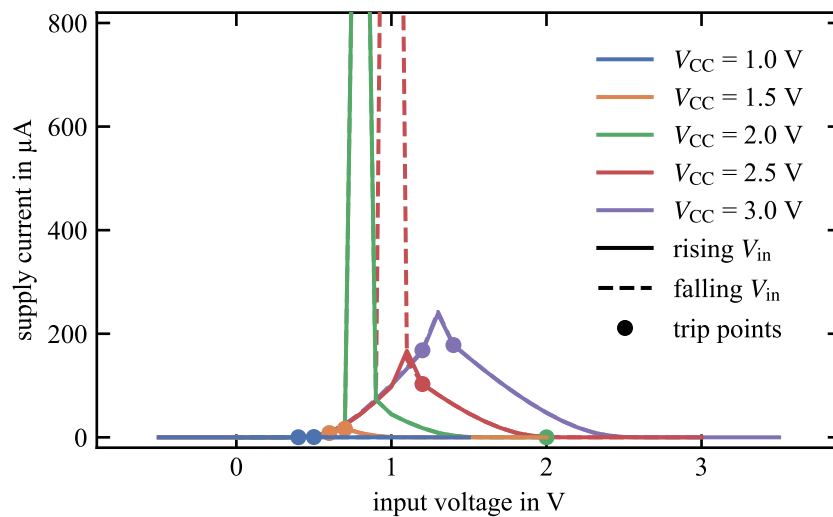


Figure 10: Measurement results for SN74AUP2G04 CMOS inverter. The $V_{CC} = 2.0$ V measurement reached a maximum of 2.0 mA. The $V_{CC} = 2.5$ V measurement reached a maximum of 3.1 mA.

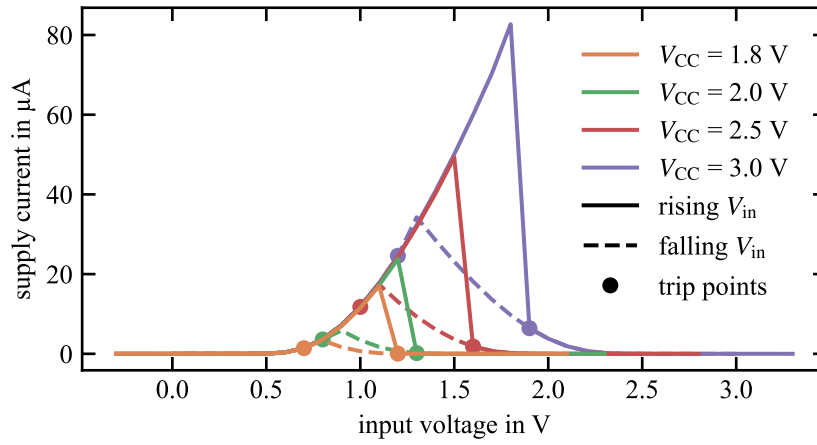


Figure 11: Measurement results for MSP430G2553 microcontroller.

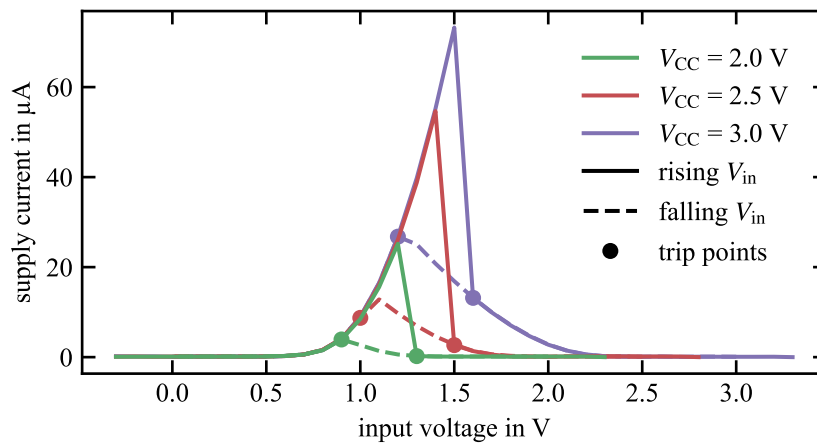


Figure 12: Measurement results for PIC12LF1572 microcontroller.

4 Shoot-Through Avoidance Circuit

The TLV3691 is the lowest quiescent supply current comparator on the market, typically 75 nA. This can be verified by several online vendor catalogs. Whenever the maximum input offset voltage of 22 mV, the hysteresis of 17 mV, and the maximum propagation delay of 45 μ s are sufficient for the application requirements, this comparator can be used. A reference voltage is required for proper operation of the comparator circuit. Depending on the application, there are generally two options, as shown in Figure 13 [FSD22].

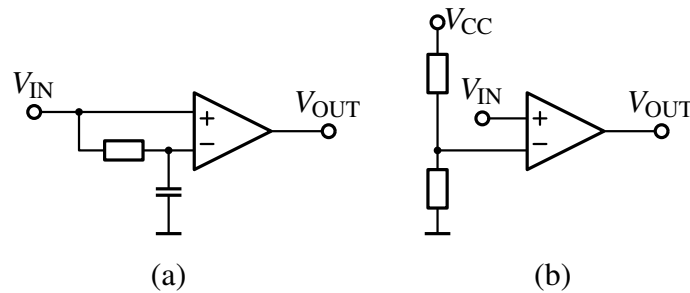


Figure 13: Proposed shoot-through avoidance circuit with (a) adaptive reference generator and (b) fixed reference.

The circuit in Figure 13a using the adaptive reference generator is preferable. It has lower power consumption and mitigates problems with input signal offsets. Such offsets can come from a bias circuit or from the input offset of an LF amplifier. However, due to its adaptive nature, only fast and DC-free input signals can be decoded. On the other hand, Figure 13b uses a fixed reference voltage generated by a resistor divider. [FSD22] The current draw of the resistor divider should be reduced by using resistor values above 10 M Ω . The reference voltage can be freely configured, but should be greater than 100 mV. This ensures that the effect of the comparator input offset is reduced. We have estimated a current flow of 100 nA through the resistor divider. Therefore, the proposed current draw is in the range of only 175 nA.

To verify that there is no STE with our proposed circuit, we repeated the STE measurements. A reference voltage of 0 V was used because the inverting input of the comparator was connected to ground. We added a 20 dB attenuator to the voltage source V_{in} to improve the accuracy. The results of this measurement are shown in Figure 14.

The comparator supply current remained constant at an average of 55 nA. No STE is visible. The trip points are at 4 mV and 15 mV. Therefore, an input offset voltage of 9.5 mV and a hysteresis of 11 mV can be calculated for this particular device.

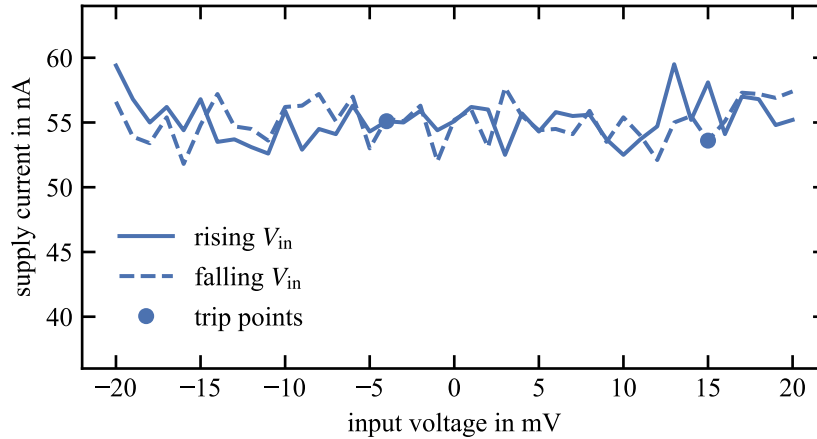


Figure 14: Measurement results for TLV3691 comparator at 3 V supply voltage.

5 Conclusion

Wireless sensor nodes can only survive for several years on a single battery charge if their power consumption is reduced to a minimum. Wake-up receivers (WuRxs) are commonly used to minimize the power consumption of the sensor node while maintaining low latency communication. The power consumption of the WuRx must remain below $10 \mu\text{W}$ to allow sufficient battery life for the sensor node. [Kan+21]

In this article we examined the so-called shoot-through effect (STE) of complementary metal-oxide-semiconductor (CMOS) logic devices. The STE is an increase in the device supply current whenever an analog signal of intermediate voltage is applied to the input of a logic device. [HH15, p. 760]

In section 2 we analyzed the state of research of commercial off-the-shelf (COTS) WuRx implementations. We found that in many circuits, analog signals are directly connected to digital logic devices. Outstanding is the preamble detector proposed in [MB14], which has been used repeatedly in over 20 articles. We have simulated this circuit and verified that an intermediate voltage is generated by the analog filter (see Figure 2 and Figure 3).

In section 3, we performed measurements to verify the STE in eight different CMOS devices: CMOS inverters and Schmitt triggers from the HC, LV, and AUP logic families. In addition, measurements were performed on the MSP430G2553 and PIC12LF1572 microcontrollers. The measurements were repeated for different supply voltages. Overall, we found significant STE currents for most devices and supply voltages. The STE current peaks ranged from $17 \mu\text{A}$ to 6.0 mA . Comparing these STE currents to the typical power consumption of a WuRx shows that STE currents can significantly reduce the battery life of the sensor node.

Note that not all WuRx-equipped sensor nodes must be affected by STE currents. Whether the STE occurs or not depends on the true input voltage of the logic device. However, this input voltage depends on many effects, such as the offset voltage of the LF amplifier, the noise level of the environment, the logic device, and the supply voltage. Nevertheless, based on our measurements, we can estimate that a fraction of the WuRx-equipped sensor nodes will be plagued by the STE and show significantly reduced battery life.

In section 4, we propose a circuit to avoid the STE. A comparator circuit with ultra-low quiescent current can be added to the circuit. We have verified by measurements that these comparators do not show signs of STE. Adding these circuits to WuRxs significantly increases reliability.

Data Availability Statement

The data presented in this study are openly available in FigShare at [10.6084/m9.figshare.25164059](https://doi.org/10.6084/m9.figshare.25164059).

References

- [Ben+22] Ahmed Abed Benbuk et al. “Tunable, Asynchronous, and Nanopower Baseband Receiver for Charging and Wakeup of IoT Devices”. In: *IEEE Internet of Things Journal* 9.4 (2022), pp. 3023–3036. DOI: 10.1109/JIOT.2021.3094881.
- [Ché+13] Rym Chéour et al. “Wireless sensor networks with power management for low energy consumption”. In: *10th International Multi-Conferences on Systems, Signals & Devices 2013 (SSD13)*. 2013, pp. 1–6. DOI: 10.1109/SSD.2013.6564161.
- [Del+16] M. Del Prete et al. “Optimum Excitations for a Dual-Band Microwatt Wake-Up Radio”. In: *IEEE Transactions on Microwave Theory and Techniques* 64.12 (2016), pp. 4731–4739. DOI: 10.1109/TMTT.2016.2622699.
- [Dji+21] Nour El Hoda Djidi et al. “Enhancing Wake-Up Receivers Reliability through Preamble Filtering and Minimum Energy Coding”. In: *2021 IEEE International Symposium on Circuits and Systems (ISCAS)*. 2021, pp. 1–5. DOI: 10.1109/ISCAS51556.2021.9401366.

- [FSD22] Robert Fromm, Lydia Schott, and Faouzi Derbel. "Improved Wake-Up Receiver Architectures with Carrier Sense Capabilities for Low-Power Wireless Communication". In: *Sensor Networks*. Ed. by Andreas Ahrens et al. Cham: Springer International Publishing, 2022, pp. 60–84. ISBN: 978-3-031-17718-7. DOI: 10.1007/978-3-031-17718-7_4.
- [Frø+19] Anders Frøytlog et al. "Design and implementation of a long-range low-power wake-up radio for IoT devices". In: *2019 IEEE 5th World Forum on Internet of Things (WF-IoT)*. 2019, pp. 247–250. DOI: 10.1109/WF-IoT.2019.8767353.
- [GFL19] Debasish Ghose, Anders Frøytlog, and Frank Y. Li. "Enabling early sleeping and early data transmission in wake-up radio-enabled IoT networks". In: *Computer Networks* 153 (2019), pp. 132–144. ISSN: 1389-1286. DOI: 10.1016/j.comnet.2019.03.002.
- [Gom+18] Andres Gomez et al. "Precise, Energy-Efficient Data Acquisition Architecture for Monitoring Radioactivity Using Self-Sustainable Wireless Sensor Nodes". In: *IEEE Sensors Journal* 18.1 (2018), pp. 459–469. DOI: 10.1109/JSEN.2017.2716380.
- [GD15] Amir Guidara and Faouzi Derbel. "A real-time indoor localization platform based on wireless sensor networks". In: *2015 IEEE 12th International Multi-Conference on Systems, Signals & Devices (SSD15)*. 2015, pp. 1–8. DOI: 10.1109/SSD.2015.7348124.
- [HH15] Paul Horowitz and Winfield Hill. *The Art of Electronics*. 3rd. USA: Cambridge University Press, 2015. ISBN: 0521809266.
- [Kan+18] Olfa Kanoun et al. "Next Generation Wireless Energy Aware Sensors for Internet of Things: A Review". In: *2018 15th International Multi-Conference on Systems, Signals & Devices (SSD)*. 2018, pp. 1–6. DOI: 10.1109/SSD.2018.8570695.
- [Kan+21] Olfa Kanoun et al. "Energy-Aware System Design for Autonomous Wireless Sensor Nodes: A Comprehensive Review". In: *Sensors* 21.2 (2021). ISSN: 1424-8220. DOI: 10.3390/s21020548.
- [LP22] Yu Luo and Lina Pu. "WUR-TS: Semi-Passive Wake-Up Radio Receiver Based Time Synchronization Method for Energy Harvesting Wireless Networks". In: *IEEE Transactions on Mobile Computing* 21.11 (2022), pp. 4172–4186. DOI: 10.1109/TMC.2021.3064374.

- [MB14] Michele Magno and Luca Benini. “An ultra low power high sensitivity wake-up radio receiver with addressing capability”. In: *International Conference on Wireless and Mobile Computing, Networking and Communications* (Nov. 2014), pp. 92–99. DOI: 10.1109/WiMOB.2014.6962155.
- [Mal+07] Mateusz Malinowski et al. “CargoNet: A low-cost micropower sensor node exploiting quasi-passive wakeup for adaptive asynchronous monitoring of exceptional events”. In: *Proceedings of the 5th international conference on Embedded networked sensor systems (SenSys '07)*. Jan. 2007, pp. 145–159. DOI: 10.1145/1322263.1322278.
- [Piy+17] Rajeev Piyare et al. “Ultra Low Power Wake-Up Radios: A Hardware and Networking Survey”. In: *IEEE Communications Surveys Tutorials* 19.4 (2017), pp. 2117–2157. DOI: 10.1109/COMST.2017.2728092.
- [Pol+22] Tommaso Polonelli et al. “An open platform for efficient drone-to-sensor wireless ranging and data harvesting”. In: *Sustainable Computing: Informatics and Systems* 35 (2022), p. 100734. ISSN: 2210-5379. DOI: 10.1016/j.suscom.2022.100734.
- [SMN20] Sebastian Lucas Sampayo, Julien Montavont, and Thomas Noël. “A Performance Study of the Behavior of the Wake-Up Radio in Real-World Noisy Environments”. In: *1st Workshop on Wake-Up radio technologies for next generation wireless communications (AWAKE), in conjunction with EWSN 2020*. EWSN '20: Proceedings of the 2020 International Conference on Embedded Wireless Systems and Networks on Proceedings of the 2020 International Conference on Embedded Wireless Systems and Networks. Lyon, France: ACM, Feb. 2020, pp. 206–211. DOI: 10.5555/3400306.3400346.